Eliott	Guenat	eliott.guenat@epfl.ch
First	*Last*	*E-mail*

Paper title Dynamic force coefficients identification on air-lubricated herringbone grooved journal bearing

Authors: Eliott Guenat, Jürg Schiffmann

Elsevier journal Mechanical Systems and Signal Processing

Transactions: Volume 136, 106498

Date of Publication: 19.11.2019

DOI: https://doi.org/10.1016/j.ymssp.2019.106498

Science direct https://www.sciencedirect.com/science/article/pii/S0888327019307198?via%3Dihub

Dynamic force coefficients identification on air-lubricated herringbone grooved journal bearing

Eliott Guenat[1], Jürg Schiffmann

Ecole Polytechnique Fédérale de Lausanne, Laboratory for applied mechanical design, Maladière 71b, CP 526, CH-2002 Neuchâtel 2

Abstract

The Narrow Groove Theory (NGT) is commonly used to simulate and design grooved gas bearing. However, measurements of dynamic force coefficients of Herringbone Grooved Journal Bearings (HGJBs) is missing, hence the validation historic NGT has never been performed, despite its importance. A test rig was built in order to identify stiffness and damping coefficients of HGJBs of a rotor perturbed by piezo-electric shakers. Results indicate that the NGT captures the qualitative behavior of HGJB well but tends to overestimate the stiffness and damping coefficients by 23 and 29% respectively. Gravity led to a eccentricity ratio in excess of 15% without significant effect. The direct damping coefficient was found to be mildly non-linear with the excitation amplitude.

Keywords: Gas Bearing, Herringbone Grooved Journal Bearing, Force coefficients, Experimental

[1]Corresponding author. Email adress: eliott.guenat@epfl.ch

Roman symbols

$\mathbf{A}$	Matrix of identification
a	Groove length
$\mathbf{b}$	vector of identification
b	Ridge length
C	Damping coefficient
D	Bearing diameter
f_{ex}	Excitation frequency
f_{rot}	Rotation frequency
h	Radial clearance
h_r	Ridge radial clearance
h_g	groove clearance
I_P	Axial inertia
I_T	Transverse inertia
K	Stiffness coefficient
L	Length, bearing axial length
L_{land}	Land length
M_r	Rotor mass
N_g	Number of grooves
x	Position of the rotor center of mass
y	Position of the rotor center of mass
Z	Impedance

Greek symbols

α	Groove aspect ratio, rotor tilt angle
β	Groove angle, rotor tilt angle
γ	Relative groove length
Δ	Uncertainty
δ	Groove depth
γ	Relative groove length
σ	Uncertainty
σ_Z	Uncertainty on the impedance
ψ	Generic degree of freedom
Ω	Angular velocity
ω	Excitation frequency

Superscripts

$\hat{}$	Complex amplitude

Subscripts

0	Nominal
A	Bearing A
B	Bearing B
ex	Excitation
$grwth$	Centrigufal growth
rot	Rotational
xx, yy	Direct
xy, yx	Cross-coupled

Acronyms

$HGJB$	Herringbone Grooved Journal Bearings
IR	Infra-Red
NGT	Narrow Groove Theory

1. Introduction

Herringbone grooved journal bearings (HGJB) are suited for the development of small-scale turbomachinery for decentralized energy conversion, including waste heat recovery [1], heat pumping [2, 3], fuel cell gas recirculation [4, 5] and fuel cell pressurization [6]. Over compliant foil bearings, this technology holds the advantages of a high stiffness and a repeatable behavior as long as manufacturing is consistent. However, the modelling tools have been only partially validated with experimental data and the proper evaluation of dynamic force coefficients is non-existent.

1.1. Nature of the issue

The Narrow Groove Theory (NGT) was pioneered by on HGJB by Vohr and Chow [7]. This theory allows to predict the overall effect of spiral grooves on the pressure field of a gas bearing without having to resolve each groove individually. Based on the Reynolds equation, it adds the assumption of an infinite number of grooves and of the local incompressibility across a groove-ridge pair [8]. A detailed overview of the different modeling approaches of grooved bearings is given by Gu et al. [9]. The NGT has been applied to the design of many HGJB-supported rotors until now, with several experimental validations published. Hirs [10] investigated the load capacity of HGJB using a grooved test rotor supported on two rolling elements bearings where the external load was applied on the floating bushing. He found a good agreement between the predictions and the experiment. Malanoski [11] ran a 38 mm HGJB-supported rotor in unloaded conditions up to 60 krpm without sign of whirl instability, in accordance with the NGT-predicted critical mass used as stability criterion [12]. Cunningham et al.[13] ran rotors similar to Malanoski's with different HGJB geometries up to 60 krpm. Several rotors showed signs of subsynchronous whirl instability, with an observed critical mass 1.5 to 3 times lower than the predicted one. The same authors [14] also studied the load capacity of these rotors up to an eccentricity ratio of 0.8, conclusing that the linearized NGT was valid at small eccentricity, but could not capture the non-linear trend of the load-displacement curve observed at high eccentricity. Stanev [15] built and successfully tested a 25.4 mm aerostatic HGJB proposed by Fleming [16] using the linearized NGT. In accordance with the theory, no sign of instability was observed. Schiffmann [2] used the linearized NGT to design 10 mm refrigerant-lubricated HGJB supporting a turbocompressor up to 210 krpm, with no sign of instability. Ognjanovic

[17] investigated the load capacity of a large 60 mm HGJB on a experimental setup comparable to Hirs' [10] and concluded that the NGT tend to overestimate the load capacity, even at low eccentricity. Wagner [5] commissioned a NGT-designed 8 mm rotor on steam-lubricated HGJBs recirculating anode gas in a Solide Oxyde Fuel Cell, with no sign of instability.

NGT has proven its empirical reliability in the design of HGJB-supported rotors, recent works are employing this theory to explore new design of grooved bearings, by using non-constant groove parameters [18], non-ideal gas lubricants [19] and combination of foil and grooved bearing [20]. While the static load capacity was measured in several occasions, the evaluation of dynamic force coefficients, common for foil gas bearings [21, 22, 23, 24], is still missing in the literature for HGJB. Two families of test apparatus are present in the literature. The first one, pioneered on gas bearings by Heshmat and Ku [25], consist of a rotor supported on two stiff bearing (often oil lubricated or on rolling elements) where the test bearing, floating on the rotor, is perturbed by a force of known amplitude. Recent applications of this approach include Wang and Kim [23] and Etras and Delgado [26] for foil and hybrid bearings respectively. The second one is a rotor supported on two test bearings, with a force imposed on the bearing bushings or the rotor itself to perturb the system. The method was pioneered on gas bearings by Fleming [27], with notable recent developments from Larsen et al. [24] for foil bearings and Le Rouzic and Arghir [28] for hybrid bearings. In all published studies, the knowledge of inertial properties of bushings is necessary to retrieve the bearing force coefficients if the force is not applied on the rotor directly, in addition to the rotor inertial properties for the second family of test setups. However, the precise knowledge of these properties can be difficult to evaluate due to the complex motion of the bushing on its compliant support (flexible blades, o-rings, etc) and can be frequency-dependent.

1.2. Goals and objectives

The objectives are to 1) propose a test rig adapted to the evaluation of dynamic force coefficients of HGJB without the knowledge of bearing bushings inertial properties, 2) measure the stiffness and damping coefficients of HGJB at different excitation frequencies and rotor speeds and compare to the linearized NGT and 3) investigate the effect of static eccentricity and excitation amplitude on the results.

1.3. Scope of the Paper

A test rig for the measurement of dynamic force coefficients of HGJBs is presented together with the theoretical background allowing the evaluation of the force coefficients from the measurements. Estimated force coefficients between 400 and 1700 Hz and rotor speed 50 and 100 krpm are presented and compared to the prediction of the linearized NGT. The orientation of the test rig is changed in order to investigate the effect of gravity on the dynamic force coefficients. Finally, the amplitude of the excitation signals used for the measurements is varied in order to investigate the non-linearity of HGJB.

2. Methodology

The identification of force coefficients is performed on a turbine-driven symmetric stainless steel rotor supported on two HGJBs, presented in Figure 1. In order to improve its tribological properties in under mixed lubrication conditions, a Diamon-Like Coating (DLC) is applied on the rotor. The rotor is hold in axial position using two aerostatic bearings acting on its ends. The journal bearing bushings, manufactured in tungsten carbide, are mounted on compliant supports (Figure 1b) in order to allow two radial degrees of freedom per bearing. Two floating piezo-electric shakers are mounted on each flexibly supported bushing in orthogonal directions impose a perturbation on the bearing. The 8 degrees of freedom of the rotor-bushing system are monitored in position using proximity capacitive probes with a overall resolution of 16 nm and a bandwidth of 8.5 kHz. The temperature of the bushings and of the rotor are measured by PT100 and infra-red temperature probes, respectively. The uncertainty on the temperatures is ± 1 K for the former and ± 0.5 K for the latter. The first bending frequency of the free rotor was evaluated at 2233 Hz using a finite element code with 1D Timoshenko beam elements. The main dimensions of the setup are shown in Fig.2. The bearing clearance was estimated by measuring the bushing and rotor diameters on 5 axial locations. Mean radial clearance and circularity errors are given in Fig.3 for the bearing under investigation. The groove depth was measured between 15 and 17 µm, with a nominal value of 16 µm. The other bearing and rotor parameters are listed in Table 1 using the nomenclature of Figure 4 as reference. The bushing can be easily removed from the assembly and changed to accommodate different diameters and bearing L/D ratios.

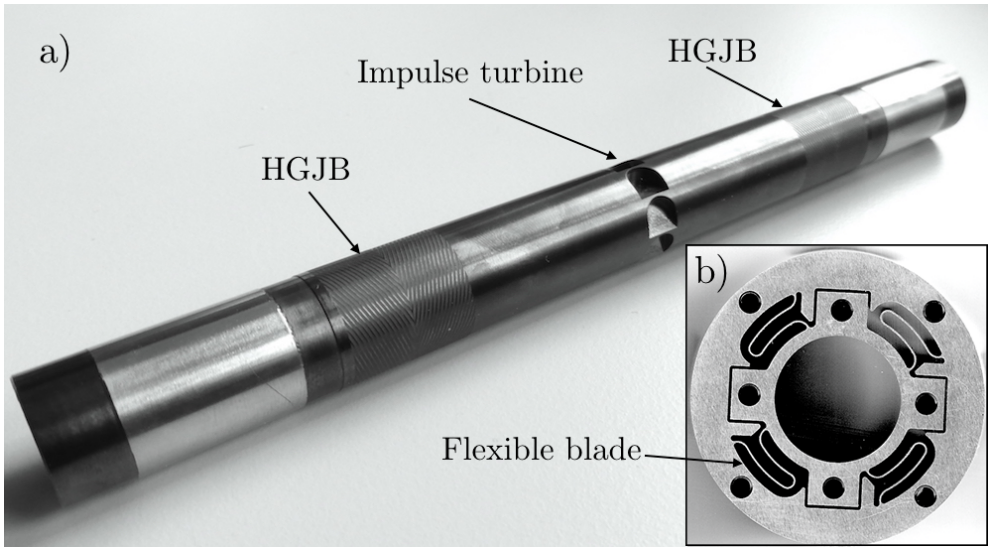

Figure 1: a) investigated rotor b) flexible bearing support

Table 1: Complementary bearing and rotor parameters

Parameter	Value
α=$a/(a+b)$	0.6
β	160°
$\gamma = L_{land}/L$	1
L/D	1
N_g	30
M_R	0.2672 kg
I_P	$8.83 \cdot 10^{-6}$ kg m^2
I_T	$7.01 \cdot 10^{-4}$ kg m^2

The relative displacement of the rotor in the bushings, as well as the absolute acceleration of the rotor, allow to retrieve the bearing force coefficients (bearing impendance $Z_{ij} = K_{ij} + \omega C_{ij}$ starting from the linearized equations of motion of the rotor in the frequency domain shown in Eq. 4 to 7 with the nomenclature indicated in Fig.5, valid for harmonic motions:

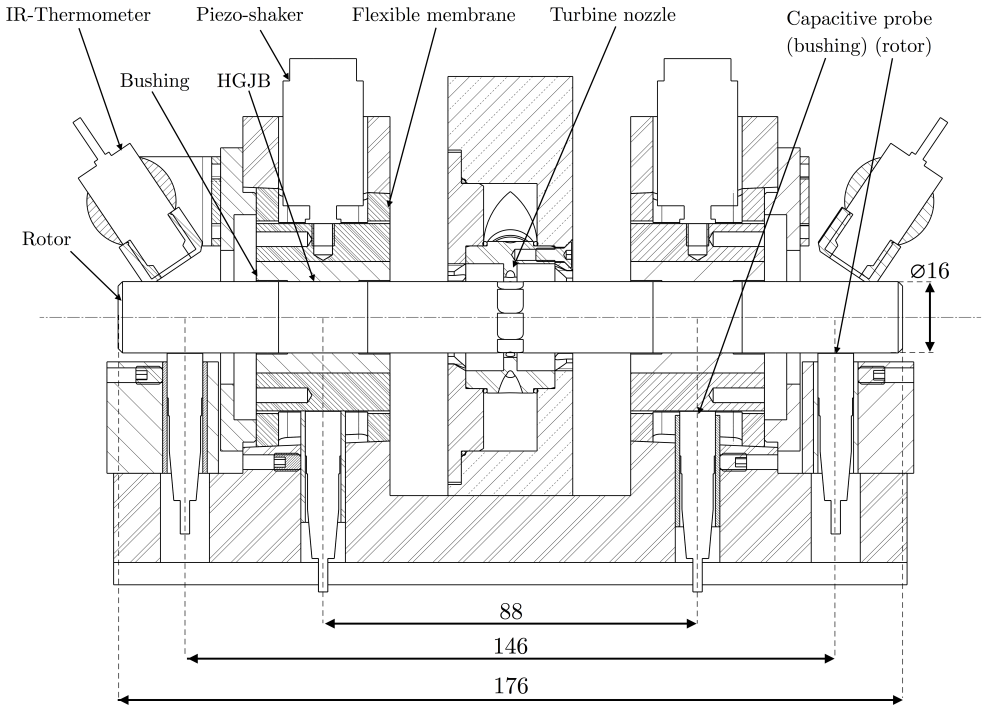

Figure 2: Cut view of the apparatus with the main dimensions

$$\psi(t) = \hat{\psi} e^{i\omega t} \tag{1}$$

$$\dot{\psi}(t) = i\omega \hat{\psi} e^{i\omega t} \tag{2}$$

$$\ddot{\psi}(t) = -\omega^2 \hat{\psi} e^{i\omega t} \tag{3}$$

where ψ denotes any of the degrees of freedom of Fig. 5.

The underlying assumptions are that 1) the rotor is rigid and 2) the bearing tilting reaction torque is small compared to the restoring torque of the linear displacement. The second assumption is justified by the center distance between the bearings: according to the linearized centered NGT, the bearings are expected to have a translational and tilting stiffness coefficients of respectively $1\,\mathrm{MN\,m^{-1}}$ and $400\,\mathrm{N\,m}$. For an arbitrary tilt angle of the rotor around its center of mass, the relative contribution of tilting stiffness in the net restoring torque is therefore less than 5%.

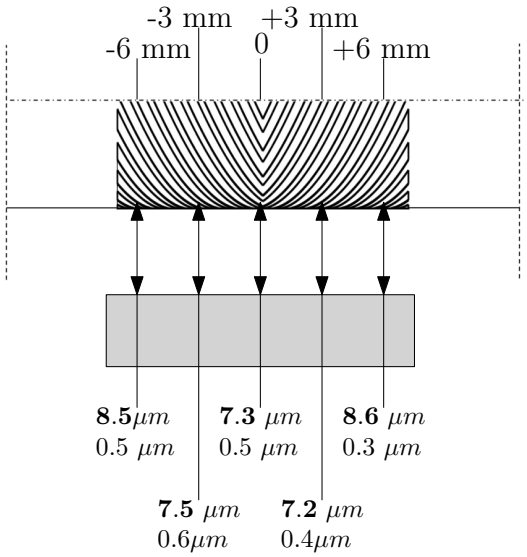

Figure 3: Measured average radial clearance (h_r) and total circularity error of both bushing and rotor in 5 axial locations at a ambient temperature of 21 °C. The bold number indicate the average radial clearance followed by the circularity error on the radial clearance

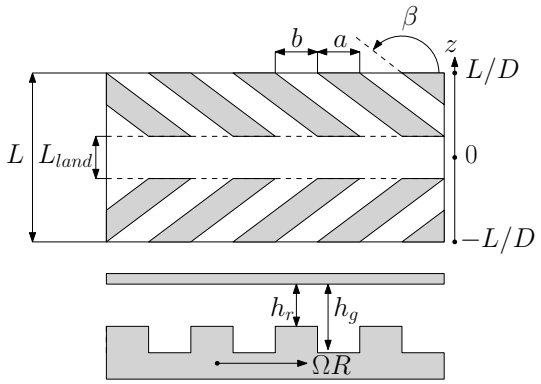

Figure 4: Nomenclature of the HGJB parameters

$$\begin{gathered} -M_R\omega^2\hat{x} \\ +Z_{xx,A}\left(\hat{x}+L_A\hat{\alpha}-\hat{x}_A\right)+Z_{xx,B}\left(\hat{x}-L_B\hat{\alpha}-\hat{x}_B\right) \\ +Z_{xy,A}\left(\hat{y}-L_A\hat{\beta}-\hat{y}_A\right)+Z_{xy,B}\left(\hat{x}+L_B\hat{\beta}-\hat{y}_B\right)=0 \end{gathered} \tag{4}$$

$$
\begin{aligned}
&-M_R\omega^2\hat{y} \\
&+Z_{yy,A}\left(\hat{y}-L_A\hat{\beta}-\hat{y}_A\right)+Z_{yy,B}\left(\hat{y}+L_B\hat{\beta}-\hat{y}_B\right) \\
&+Z_{yx_A}\left(\hat{x}+L_A\hat{\alpha}-\hat{x}_A\right)+Z_{yx_B}\left(\hat{x}-L_B\hat{\alpha}-\hat{x}_B\right)=0
\end{aligned} \tag{5}
$$

$$
\begin{aligned}
&-I_T\omega^2\hat{\alpha}-I_P i\omega\hat{\beta}\Omega \\
&+Z_{xx,A}L_A\left(\hat{x}+L_A\hat{\alpha}-\hat{x}_A\right)-Z_{xx,B}L_B\left(\hat{x}-L_B\hat{\alpha}-\hat{x}_B\right) \\
&+Z_{xy,A}L_A\left(\hat{y}-L_A\hat{\beta}-\hat{y}_A\right)-Z_{xy,B}L_B\left(\hat{y}+L_B\hat{\beta}-\hat{y}_B\right)=0
\end{aligned} \tag{6}
$$

$$
\begin{aligned}
&-I_T\omega^2\hat{\beta}+I_p i\omega\hat{\alpha}\Omega \\
&-Z_{yy,A}L_A\left(\hat{y}-L_A\hat{\beta}-\hat{y}_A\right)+Z_{yy,B}L_B\left(\hat{y}+L_B\hat{\beta}-\hat{y}_B\right) \\
&-Z_{yx,A}L_A\left(\hat{x}+L_A\hat{\alpha}-\hat{x}_A\right)+Z_{yx,B}L_B\left(\hat{x}-L_B\hat{\alpha}-\hat{x}_B\right)=0
\end{aligned} \tag{7}
$$

The 8 unknowns of the equations of motion are the four complex impedances of each bearing ($Z_{ij,A}$ and $Z_{ij,B}$). They are isolated to build Equation 8, where $\mathbf{A}$ and $\mathbf{b}$ are the matrix containing the contribution of relative displacement and the vector containing contributions of rotor acceleration and gyroscopic effects. Two linearly independent test runs are necessary per evaluation for a unique non trivial solution to the system to exist, justifying the use of four shakers in order to excite the system in two orthogonal directions. It is remarkable that this method requires neither the knowledge of inertial parameters of the bearing bushings nor of any force measurement.

$$
\mathbf{A}\cdot\begin{pmatrix} Z_{xx,A} & Z_{xy,A} & Z_{yy,A} & Z_{yx,A} & Z_{xx,B} & Z_{xy,B} & Z_{yy,B} & Z_{yx,B} \end{pmatrix}^T=\mathbf{b} \tag{8}
$$

The present method holds a major advantage over the existing approaches for the measurement of force coefficients, since it does not require the knowledge of mass and inertia of bearing bushings nor the measurement of any force, but instead relies solely on the position measurement of the rotor and bushings, with an arbitrary force applied on the bushings. Only the knowledge of the inertial properties of the rotor are necessary, which is inherent to the floating rotor configuration. The computed eigenfrequencies of the system corresponding to Figure 5 are displayed in Fig. 6. The system operates beyond the critical speeds, however without any fundamental consequence

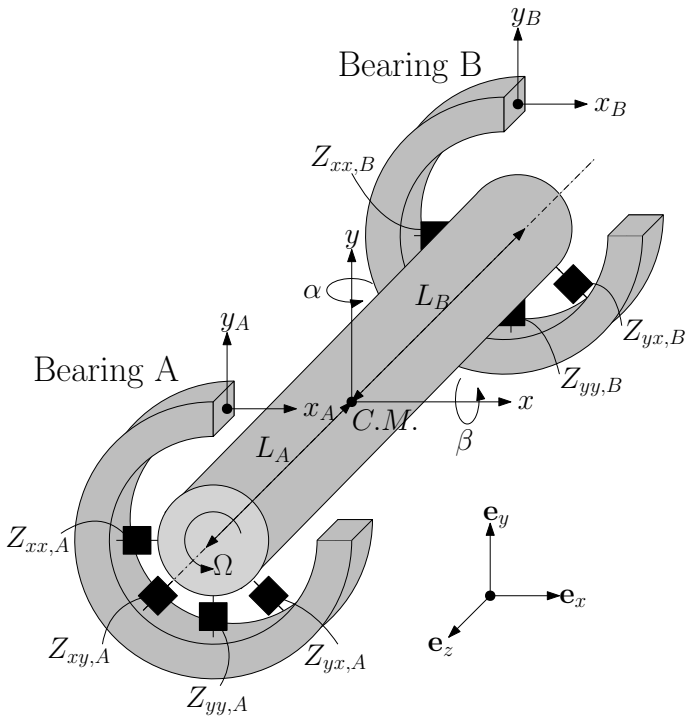

Figure 5: Nomenclature and coordinates of the rotating shaft supported on two gas bearings. C.M. denotes the center of mass, (x_A, y_A) and (x_B, y_B) the respective position of the bushings, (x, y) the position of the center of mass and (α, β) the tilt angle of the rotor. L_A and L_B denote the distances between the respective bearings and the center of mass

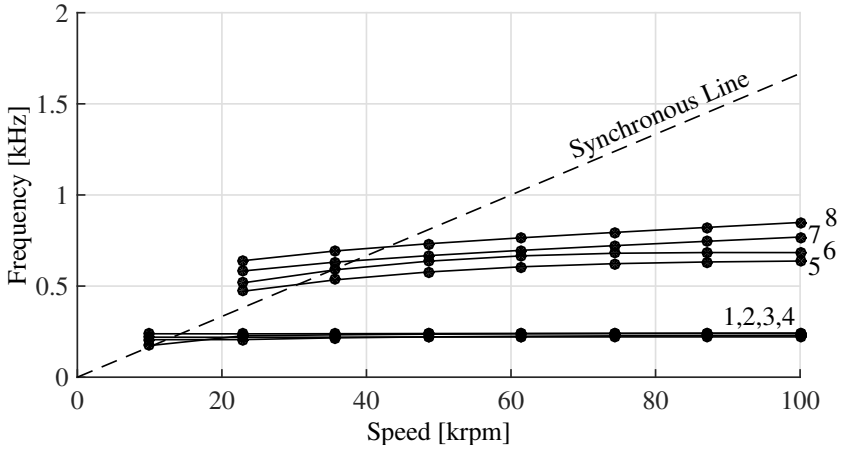

Figure 6: Computed eight eigenfrequencies as a function of rotor speed

on the identification of the dynamic force coefficients, since the procedure is independent of the sub- or super-critical nature of the dynamic system.

Each test run is performed as follows: 1) Acceleration of the rotor up to its target speed within 100 krpm. 2) A first pair of co-planar shakers is actuated for 4 seconds with a sine wave at the excitation frequency f_i. 3) The rotor runs for 30 seconds without excitation 4) The second pair of co-planar shakers is actuated for 4 seconds with a sine wave at the excitation frequency f_i. 5) Repetition steps 2) and 3) with the next excitation frequency. 6) Coast down.

Imposed excitation signals range from 400 to 1700 Hz with a 100 Hz interval, in order to be higher than the low-frequency noise generated by the turbine (as visible in Fig. 9) but well under the first rotor bending frequency. The signal of each excitation is processed by applying a band filter around the nominal excitation frequency and a sine wave fit is performed on the resulting signal to extract its frequency, amplitude and phase. The results are compared to the predictions of the perturbed NGT at concentric position [7], taking into account the deviation in the clearance and groove depth measurements. The measurement uncertainty accounts for the resolution, precision and accuracy of the capacitive probes and their measurement chain, the uncertainties on the rotor mass, intertias and spacial positions and the uncertainties appearing during the signal processing (band gap filter and time-domain identification [29]). The latter are estimated numerically by constructing a reference signal polluted with different levels of pseudo-white noise, processing the signal and comparing the identified phase, amplitude and frequency to the reference. The procedure results in a look-up table allowing to recover the uncertainty on the amplitude and the phase from the signal-to-noise ratio, evaluated by comparing the estimated amplitude of the signal to the background noise in the vicinity of the corresponding frequency. The uncertainties of all N parameters are then combined with Eq. 9, with the differential term evaluated numerically with a finite-difference scheme:

$$\sigma_{Z_j} = \sqrt{\sum_{i=1}^{N} \left(\frac{\partial Z_j}{\partial x_i} \sigma_i \right)^2} \tag{9}$$

where Z_j designates any component of the impedance vector of Equation 8 and x_i any of the N parameters involved in the estimation of Z_j.

The experimental results are compared to the numerical predictions from the NGT. The non-linear differential equation is linearized around the centered position with the perturbation technique of Lund [12], as developed in [19].

3. Results and discussion

Figure 7 shows the evolution of the rotor speed between ramp-up, steady operation and coast-down. The evolution of the corresponding rotor and bearing temperatures is shown in Fig. 8. The temperature evolution is taken into account in the model predictions of force coefficients, since the difference in thermal expansion coefficients between bushing and rotor results in a change of clearance. The centrifugal radial growth of the rotor is computed with Eq.10 and reaches 0.38 µm at 100 krpm. Figure 9 represents the evolution of the spectrum in time, measured by one of the rotor proximity probes. The synchronous whirl is visible, as well as a persistent sub-synchronous noise around 300 Hz. This noise is is induced by the impulse turbine, since it vanishes as the rotor initiates its coast-down (turbine air cut). The piezo-shakers excitation signals are visible in pairs at each excitation frequency. The evolution of the maximal orbit amplitude of the rotor at the bearing locations is shown in Fig. 10. At nominal speed, the orbit due to residual unbalance uses between 9 and 13% of the bearing clearance. The maximum compressibility number is 12.8 based on the average radial clearance.

$$\Delta h_{grwth} = \frac{\rho(1-\nu)\Omega^2 R^2}{12} \tag{10}$$

The identified stiffness and damping coefficients under vertical rotor operation are presented in Fig.11 and 12 respectively for a rotor speed of 100 krpm ($\Lambda = 13.43$) and compared with the NGT-based model. The three categories of prediction are based on the average clearance, the clearance with the average circularity error and the extreme values, as detailed in Table 2. The 4 pairs of dynamic force coefficients exhibit a high degree of isotropy, as the difference between corresponding coefficients in orthogonal directions are not significantly different. The frequency-dependency of the force coefficients is qualitatively captured by the predictions, although the model slightly overestimates the value of stiffness and damping coefficients. The predictions based on the largest measured clearance gives the best agreement with the

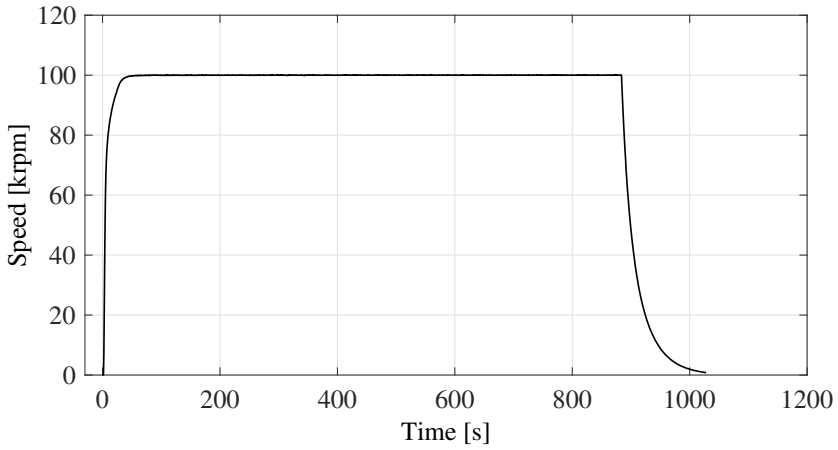

Figure 7: Evolution of rotor speed for the measurements at 100 krpm

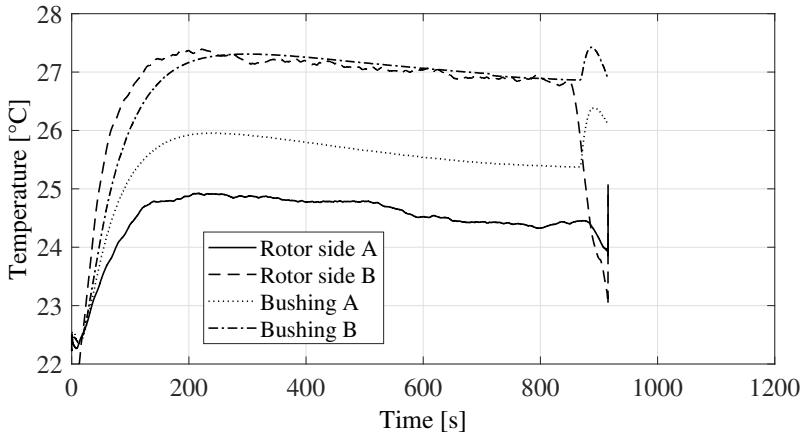

Figure 8: Evolution of rotor and bushing temperatures for the measurements at 100 krpm

estimated parameters. At low excitation frequency, the measurements of the direct stiffness and damping coefficient are respectively 31 and 40% lower than the NGT prediction based on the average clearance. The evaluation of the cross-coupled damping coefficient is the most affected by uncertainties, while the direct stiffness enjoys a good robustness against uncertainties. The direct stiffness starts with a plateau close to the static value and experiences a progressive increase toward a second higher plateau at larger relative excitation frequency. The first plateau and the rise are observed experimentally whereas the second plateau is beyond the maximum excitation frequency.

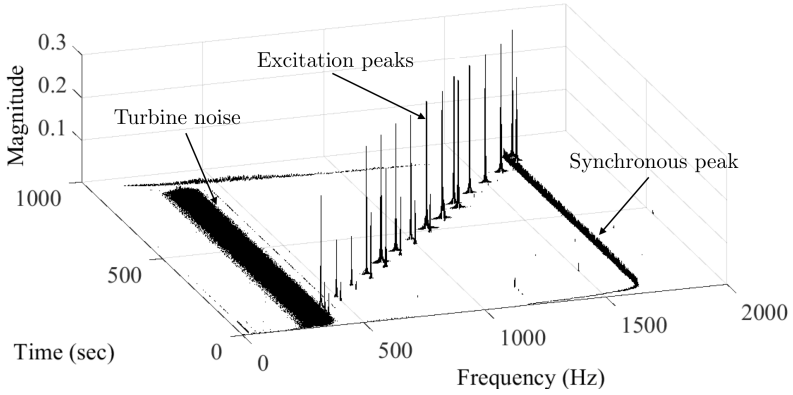

Figure 9: Spectrum of the measurement run at 100 krpm in waterfall view

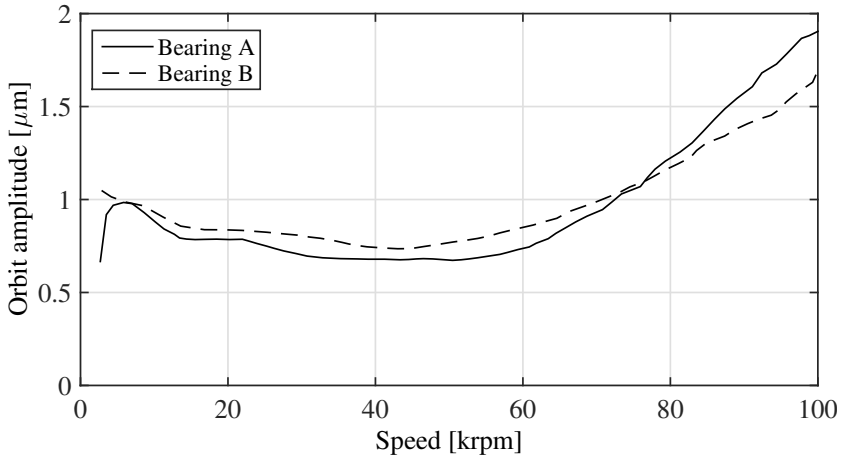

Figure 10: Total orbit amplitudes for both bearings as a function of rotor speed during the acceleration

The cross-coupled stiffness first slowly decreases and experiences a recovery with raising excitation frequency. The direct damping coefficients exhibit a nearly constant value over the investigated range of excitation frequency, which is predicted by the NGT based on the largest clearance. Finally, the cross-coupled damping coefficients have a inflexion point predicted at $f_{ex}/f_{rot} \approx 0.65$, which is hardly noticeable experimentally because of the large uncertainties affecting the identified values. However, the prediction based on the largest clearance offers a good match with the data. The uncertainties on the prediction generally grow with the excitation frequency.

Table 2: Clearance and groove depth used for the prediction of dynamic force coefficients corresponding to the legend of Fig.11 to 14. δ_0=16 µm, $\Delta\delta$ =1 µm

	h_0	δ
Model Nominal	$\frac{1}{5}\sum_{i=1}^{5}\bar{h}_i$	δ_0
Mean deviation	$\frac{1}{5}\sum_{i=1}^{5}(\bar{h}_i \pm \Delta h_i)$	δ_0
Max deviation	$\max_i / \min_i(\bar{h}_i \pm \Delta h_i)$	$\delta_0 \pm \Delta\delta$

A comparable agreement is observed at half the nominal speed, namely 50 krpm (Λ= 6.72), as shown in Fig.13 and 14. The relative deviation of the predictions at average clearance on the direct stiffness and damping coefficients at low frequency is approximately 38 and 27% respectively. The trend of all four dynamic coefficients toward higher relative excitation frequencies is well captured. The good qualitative agreement between the measured force coefficients and the ones predicted by the NGT-based model is remarkable, considering the very strong assumptions made for obtaining this simplified model (1. infinite number of grooves, 2. local incompressibility across a groove-ridge pair and 3. linearization of the modified Reynolds equation by the perturbation analysis)

Effect of excitation amplitude

The method of perturbation used to predict the bearing linear dynamic force coefficients is strictly valid only for infinitesimal displacement around the equilibrium position and does not capture non-linearities in the bearings dynamic behavior. In order to appreciate the linear behavior of the HGJB experimentally, the amplitude of the excitation signal imposed on the shakers is progressively increased, leading to a larger displacement of the rotor relative to the bushing, deviating increasingly from the infinitesimal perturbation. Results for a rotor speed of 70 krpm ($\Lambda = 9.40$) are shown in Fig. 15 and 16, with the estimated force coefficients at $f_{ex} = 700$ and 900 Hz evaluated at different amplitude of relative displacement. An evolution of the force coefficients with the amplitude of displacement is significant only on the direct damping, although in very modest proportions for the investigated excitation amplitudes. This indicates that the HGJB has, in general, a linear dynamic behavior around the unloaded position, although the mentioned

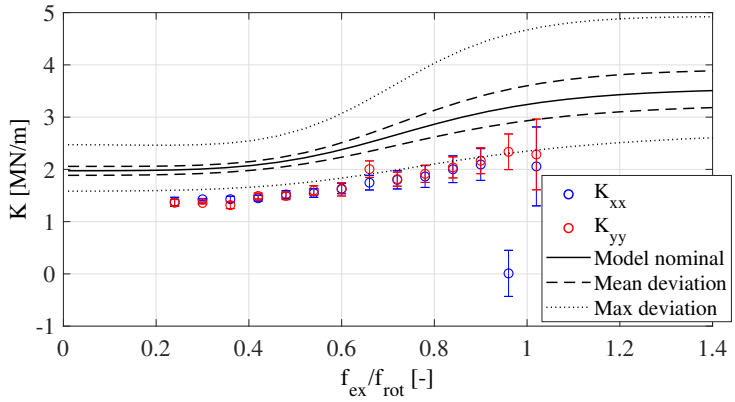

a) Direct stiffness

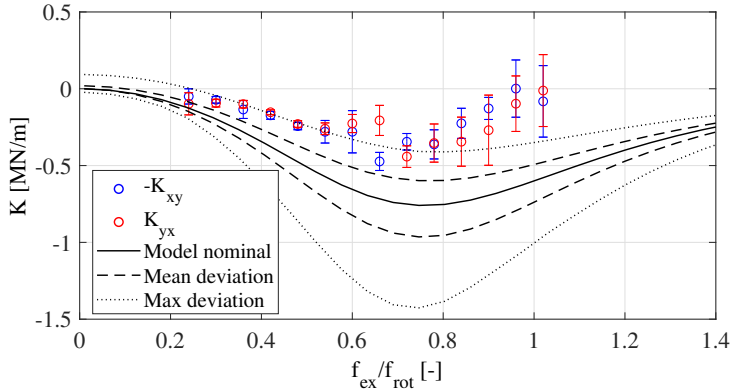

b) Cross-coupled stiffness

Figure 11: Results of identified stiffness coefficients at 100 krpm in ambient air in a vertical configuration

dynamic coefficient is prone to non-linearity when the relative displacement becomes large. It is interesting to note that the measurement uncertainty decreases with the excitation amplitude. Hence there is a trade-off between accurate measurements and the avoidance of triggering the non-linearities of the bearing force coefficients. The evaluations shown in Fig. 11 to 14 were performed with a radial displacement in the order of 1 µm, which offers a good trade-off between a low uncertainty on the estimated coefficients and the influence of non-linearities.

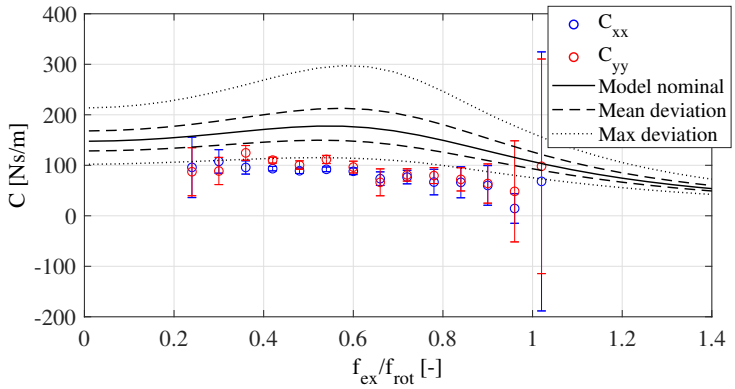

a) Direct damping

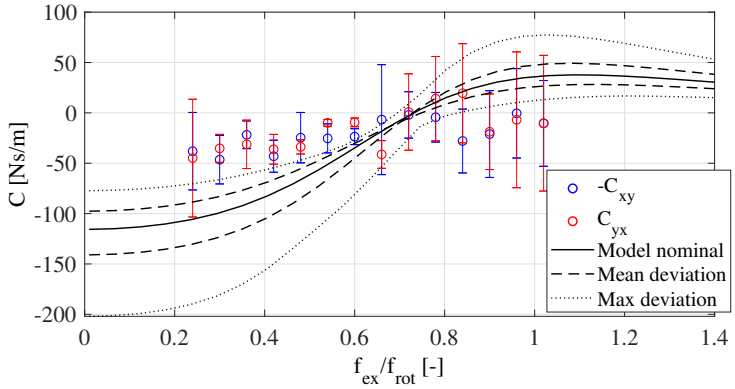

b) Cross-coupled damping

Figure 12: Results of identified damping coefficients at 100 krpm in ambient air

Influence of weight

In order to highlight changes in the dynamic force coefficients due to the static eccentricity the test rig position was changed from vertical to horizontal and measurements are repeated at half the nominal speed. The static load on each bearing is 1.3 N in the y direction, referring to the axis of Fig. 5. The difference in bearing and rotor temperature between the two tests were negligible. The center of the rotor shifted by 1.5 µm compared to the vertical unloaded position, which, assuming the vertical position as the center of the bearing, corresponds to an eccentricity ratio between 15.1 and 22.0 % (with the clearance reported in Fig.3). The estimated dynamic force coefficients are compared in Fig. 17 and 18, showing K_{yy}, K_{xy}, C_{yy} and C_{xy}. The plot clearly suggests that the static load does not lead to any significant difference

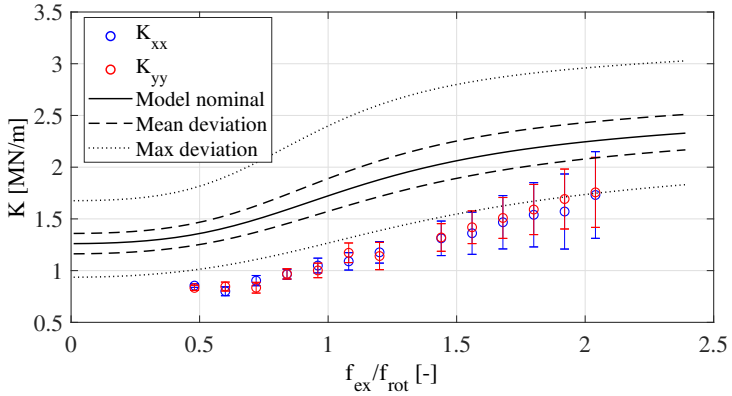

a) Direct stiffness

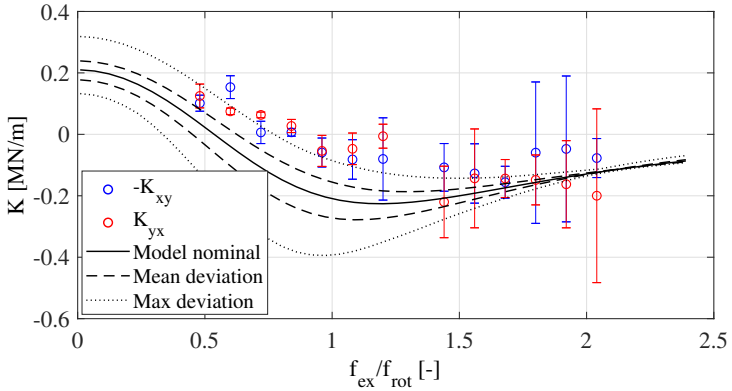

b) Cross-coupled stiffness

Figure 13: Results of identified stiffness coefficients at 50 krpm in ambient air

in the measured force coefficients for $\epsilon < 0.15$.

4. Conclusions

In order to assess the dynamic predictions of the Narrow Groove Theory commonly employed in the design of spiral groove bearings, a test rig consisting in a rotor supported on two Herringbone grooved journal bearings and excited with shakers was built. Dynamic force coefficient were estimated experimentally at different speeds, orientation with respect to gravity and excitation amplitudes. The following observations follow the experimental campaign:

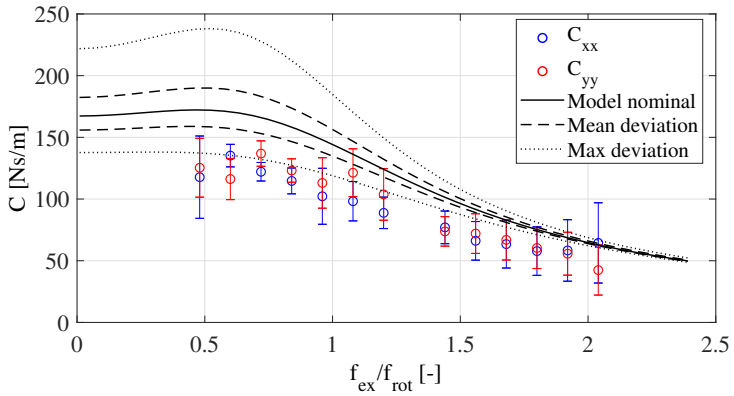

a) Direct damping

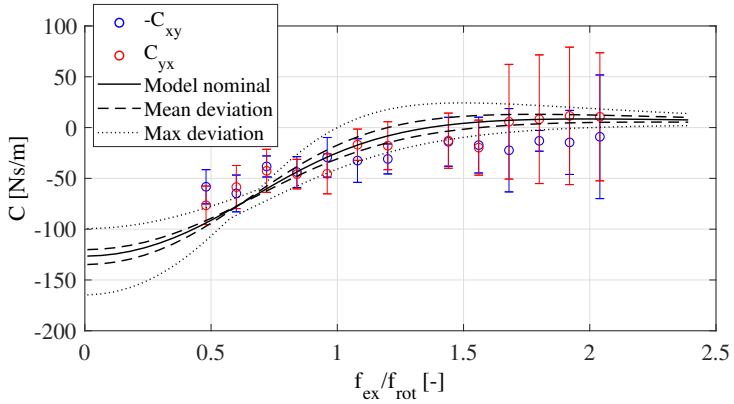

b) Cross-coupled damping

Figure 14: Results of identified damping coefficients at 50 krpm in ambient air

- Estimation of bearing dynamic force coefficient are possible on a floating rotor without force measurements
- The stiffness and damping coefficients predicted by the linearized NGT are in good qualitative agreement with the measured values
- The NGT tend to overestimate the stiffness and damping of HGJBs. At nominal speed, direct stiffness and damping coefficients were measured 38% and 27% lower than the NGT prediction with average clearance.
- Static eccentricity has little influence on the bearing dynamic force coefficients at least up to 15% eccentricity ratio.

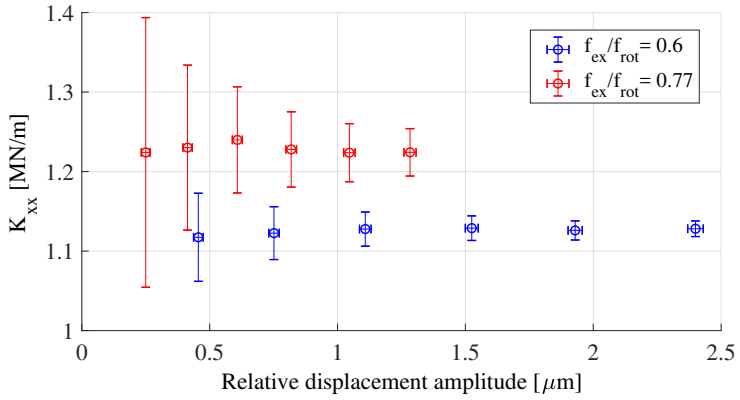

a) Direct stiffness

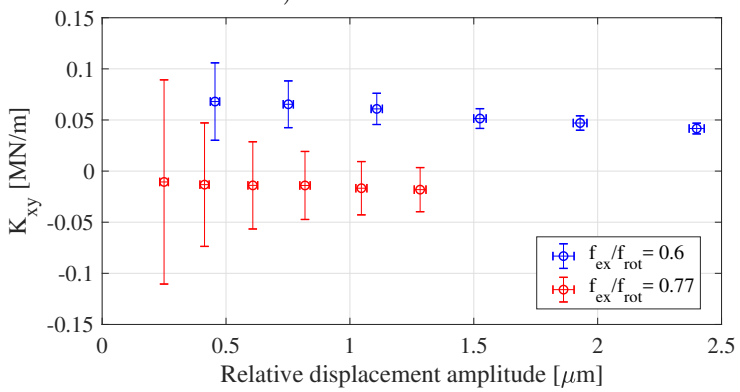

b) Cross-coupled stiffness

Figure 15: Results of identified stiffness coefficients at 70 krpm in ambient air

- The direct damping coefficient shows a modest dependency on the excitation amplitude, indicating a non-linear behavior. The other dynamic coefficients were found not found significantly sensitive to the excitation amplitude, suggesting a linear behavior.

- The comparison between the experimental and the model-based data suggests that the dynamic force coefficients are very sensitive to the bearing clearance and as a consequence also to manufacturing deviation. The results seem to suggest that the maximum clearance is the dominating value for best agreement.

The method and the results presented in this work provide a first validation of the NGT as a design and investigation tool for predicting the dynamic

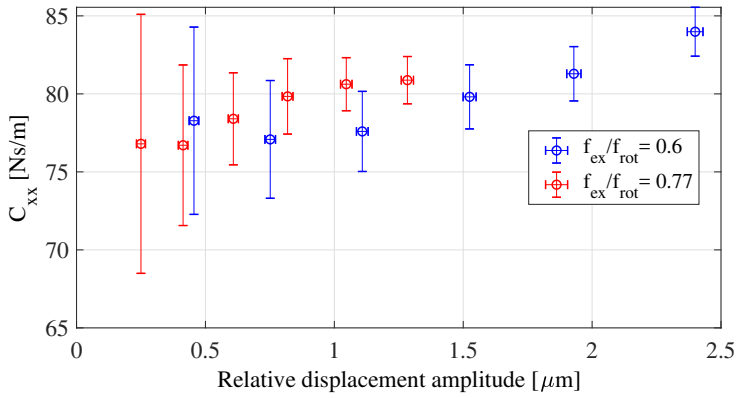

a) Direct damping

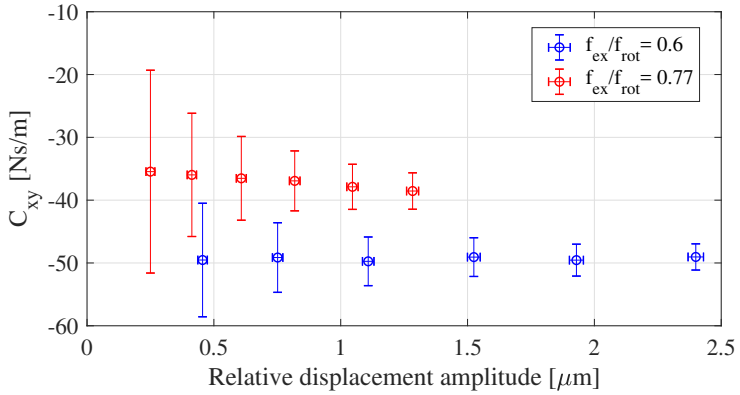

b) Cross-coupled damping

Figure 16: Results of identified stiffness coefficients at 70 krpm in ambient air

force coefficients of grooved gas bearings. They also shed light upon the limitation of the theory to predict the dynamic behavior quantitatively, which should be taken into account when designing a system based on the NGT.

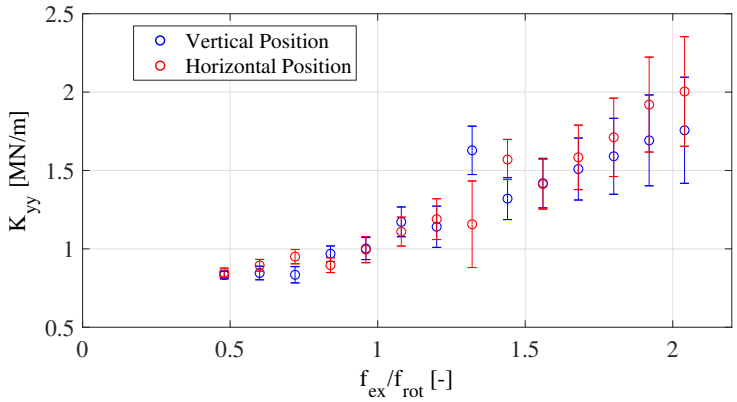

a) Direct stiffness

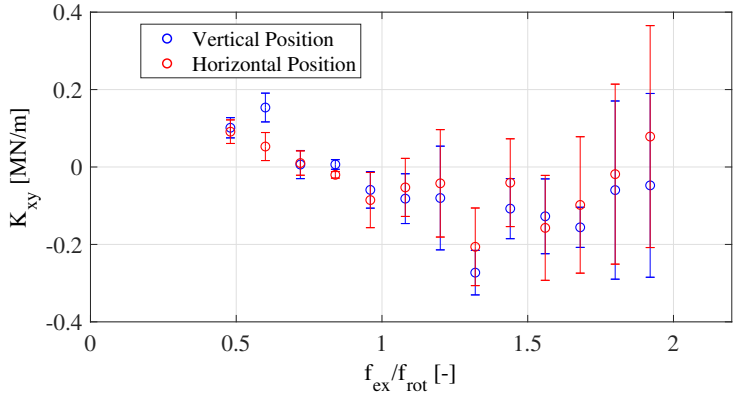

b) Cross-coupled stiffness

Figure 17: Comparison of identified dynamic stiffness coefficients at 50 krpm and different orientations

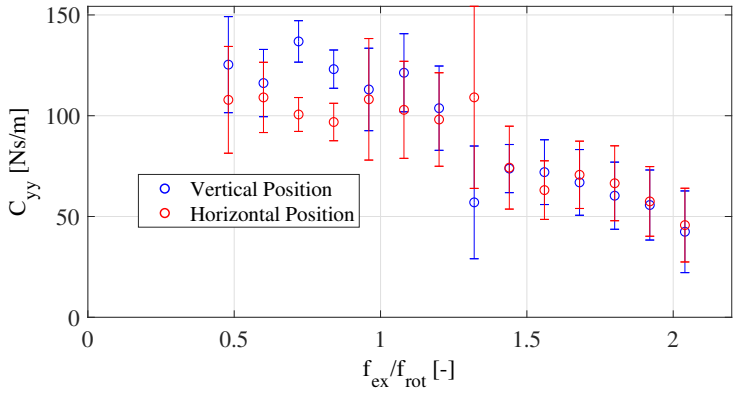

a) Direct damping

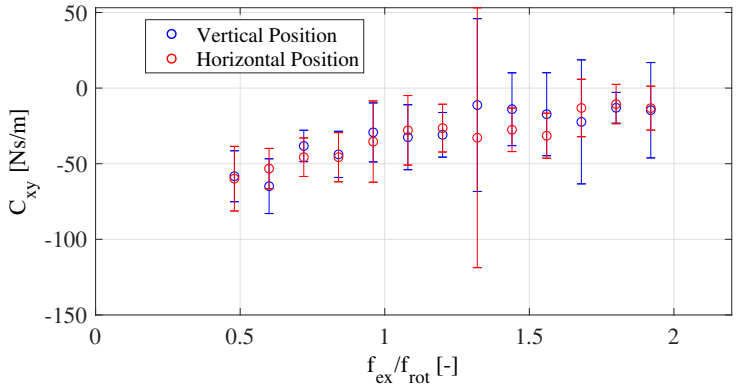

b) Cross-coupled damping

Figure 18: Comparison of identified dynamic damping coefficients at 50 krpm and different orientations

Reference

[1] K. Rosset, V. Mounier, E. Guenat, J. Schiffmann, Multi-objective optimization of turbo-ORC systems for waste heat recovery on passenger car engines, Energy 159 (2018) 751–765. doi:10.1016/j.energy.2018.06.193.

[2] J. Schiffmann, D. Favrat, Experimental investigation of a direct driven radial compressor for domestic heat pumps, International Journal of Refrigeration 32 (8) (2009) 1918–1928. doi:10.1016/j.ijrefrig.2009.07.006.

[3] J. Schiffmann, D. Favrat, Integrated design and optimization of gas bearing supported rotors, Journal of Mechanical Design 132 (5) (2010) 051007. doi:10.1115/1.4001381.

[4] P. H. Wagner, Z. Wuillemin, S. Diethelm, J. Van herle, J. Schiffmann, Modeling and designing of a radial anode off-gas recirculation fan for solid oxide fuel cell systems, Journal of Electrochemical Energy Conversion and Storage 14 (1) (2017) 011005. doi:10.1115/1.4036401.

[5] P. H. Wagner, Integrated design, optimization, and experimental realization of a steam-driven micro recirculation fan for solid oxide fuel cell systems, PhD Thesis, Ecole Polytechnique Fdrale Lausanne (EPFL), Switzerland.doi:10.5075/epfl-thesis-9337.

[6] D. Zhao, B. Blunier, F. Gao, M. Dou, A. Miraoui, Control of an ultrahigh-speed centrifugal compressor for the air management of fuel cell systems, IEEE Transactions on Industry Applications 50 (3) (2014) 2225–2234. doi:10.1109/TIA.2013.2282838.

[7] J. H. Vohr, C. Y. Chow, Characteristics of herringbone-grooved, gas-lubricated journal bearings, Journal of Basic Engineering 87 (3) (1965) 568–576. doi:10.1115/1.3650607.

[8] V. N. Constantinescu, V. Castelli, On the local compressibility effect in spiral-groove bearings, Journal of Lubrication Technology 91 (1) (1969) 79–86. doi:10.1115/1.3554902.

[9] L. Gu, E. Guenat, J. Schiffmann, A Review Of Grooved Dynamic Gas Bearings, Applied Mechanics Reviewsdoi:10.1115/1.4044191.
URL https://doi.org/10.1115/1.4044191

[10] G. G. Hirs, The load capacity and stability characteristics of hydrodynamic grooved journal bearings, A S L E Transactions 8 (3) (1965) 296–305. doi:10.1080/05698196508972102.

[11] S. B. Malanoski, Experiments on an ultrastable gas journal bearing, Journal of Lubrication Technology 89 (4) (1967) 433–438. doi:10.1115/1.3617021.

[12] J. W. Lund, Calculation of stiffness and damping properties of gas bearings, Journal of Lubrication Technology 90 (4) (1968) 793–803. doi:10.1115/1.3601723.

[13] R. E. Cunningham, D. P. Fleming, W. J. Anderson, Experimental stability studies of the herringbone-grooved gas-lubricated journal bearing, Journal of Lubrication Technology 91 (1) (1969) 52–57. doi:10.1115/1.3554896.

[14] R. E. Cunningham, D. P. Fleming, W. J. Anderson, Experimental load capacity and power loss of herringbone grooved gas lubricated journal bearings, Journal of Lubrication Technology 93 (3) (1971) 415–422. doi:10.1115/1.3451610.

[15] P. T. Stanev, F. Wardle, J. Corbett, Investigation of grooved hybrid air bearing performance, Proceedings of the Institution of Mechanical Engineers, Part K: Journal of Multi-body Dynamics 218 (2) (2004) 95–106. doi:10.1243/146441904323074558.

[16] D. P. Fleming, Steady-State And Stability Analysis Of Externally Pressurized Gas-Lubricated Journal Bearings With Herringbone Grooves, NASA Report TN D-5870 (1970) 43.

[17] I. Ognjanovic, Experimental contribution to the mechanics of herringbone grooved journal air bearings, PhD Thesis, Ecole Polytechnique Fdrale Lausanne (EPFL), Switzerland.doi:10.5075/epfl-thesis-4879.

[18] J. Schiffmann, Enhanced groove geometry for herringbone grooved journal bearings, Journal of Engineering for Gas Turbines and Power 135 (10) (2013) 102501. doi:10.1115/1.4025035.

[19] E. Guenat, J. Schiffmann, Real-gas effects on aerodynamic bearings, Tribology International 120 (2018) 358–368. doi:10.1016/j.triboint.2018.01.008.

[20] E. Guenat, J. Schiffmann, Performance potential of gas foil thrust bearings enhanced with spiral grooves, Tribology International 131 (2019) 438–445. doi:10.1016/j.triboint.2018.11.003.

[21] C. Dellacorte, Stiffness and damping coefficient estimation of compliant surface gas bearings for oil-free turbomachinery, Tribology Transactions 54 (4) (2011) 674–684. doi:10.1080/10402004.2011.589966.

[22] L. San Andrs, T. A. Chirathadam, Metal mesh foil bearing: Effect of motion amplitude, rotor speed, static load, and excitation frequency on force coefficients, Journal of Engineering for Gas Turbines and Power 133 (12) (2011) 122503. doi:10.1115/1.4004112.

[23] Y. P. Wang, D. Kim, Experimental Identification of Force Coefficients of Large Hybrid Air Foil Bearings, in: Proceedings of ASME Turbo Expo 2013: Turbine Technical Conference and Exposition, ASME, San Antonio, Texas, USA, 2013, p. 10. doi:10.1115/GT2013-95765.

[24] J. S. Larsen, A. J. T. Hansen, I. F. Santos, Experimental and theoretical analysis of a rigid rotor supported by air foil bearings, Mechanics & Industry 16 (1) (2015) 106. doi:10.1051/meca/2014066.

[25] H. Heshmat, C.-P. R. Ku, Structural Damping of Self-Acting Compliant Foil Journal Bearings, Journal of Tribology 116 (1) (1994) 76. doi:10.1115/1.2927050.

[26] B. Ertas, A. Delgado, Compliant Hybrid Gas Bearing Using Modular Hermetically Sealed Squeeze Film Dampers, Journal of Engineering for Gas Turbines and Power 141 (2) (2019) 022504. doi:10.1115/1.4041310.

[27] D. P. Fleming, W. J. Thayer, R. E. Cunningham, Dynamic Stiffness and Damping of Externally Pressurized Gas Lubricated Journal Bearings, Journal of Lubrication Technology 99 (1) (1977) 101. doi:10.1115/1.3452954.

[28] J. Le Rouzic, M. Arghir, Experimental Analysis of Angled Injection Aerostatic Hybrid Bearings, Journal of Engineering for Gas Turbines and Power 140 (2) (2017) 022504. doi:10.1115/1.4037873.

[29] F. C. Alegria, A. C. Serra, Uncertainty of the estimates of sine wave fitting of digital data in the presence of additive noise, in: 2006 IEEE Instrumentation and Measurement Technology Conference Proceedings, IEEE, 2006, pp. 1643–1647. doi:10.1109/IMTC.2006.328187.